Available online at www.sciencedirect.com
SCIENCE DIRECT®
Journal of the European Ceramic Society 25 (2005) 3097–3107
www.elsevier.com/locate/jeurceramsoc

A study on the fundamental ceramic–polymer interactions in the high CeO_2-loading polyethylene glycol blend

Xiong Yin[a], Liang Hong[a,b,*], Zhaolin Liu[b]

[a] *Department of Chemical and Biomolecular Engineering, National University of Singapore, Blk E5 02-02, 4 Engineering Drive 4, Singapore 117576, Singapore*
[b] *Institute of Materials Research & Engineering, 3 Research Link, Singapore 117602, Singapore*

Received 8 May 2004; received in revised form 18 September 2004; accepted 24 September 2004

Abstract

Rheology of a polymer melt including ceramic particles is far cry from that of the pristine polymer phase because of the interactions between polymer and ceramic particles. This work focuses on the flow behavior of the blend comprising polyethylene glycol (PEG) melt and a fine powder (size <5 μm) of cerium(IV) oxide under low shear rates. The blend containing as high as 80 wt.% (or 41.6 vol.%) of CeO_2 can still exhibit Bingham plastic response in the low shear rate range. Hence, the relative viscosities (η_{rel}) of the PEG–CeO_2 mixtures with various volume fractions of CeO_2 (ϕ) could be obtained at different temperatures, and these data were then used to simulate the rheological model developed in this work. This model was created by assuming that there are two primary forces governing the rheological behavior of the blend, which are the van der Waals attractive forces that exist among CeO_2 particles and the chemical adsorption of PEG segments on CeO_2 particles, respectively. The simulation turns out that this model matches more precisely the changes of η_{rel} versus ϕ at different temperatures than the three widely quoted models. Furthermore, the occurrence of the two stipulated forces in the PEG–CeO_2 blend has also been verified by other experimental evidences, e.g. scanning electron microscopy (SEM), X-ray diffraction (XRD), FTIR, and differential scanning calorimetry (DSC).

Keywords: Composite; Mixing; Rheology; CeO_2; Membranes

1. Introduction

Porous ceramic membranes have been widely used for executing various filtration processes[1–3] and for facilitating operations of chemical or biological reactors[4–8] because of their remarkable chemical and thermal stability[7] in addition to extraordinary dimensional stability. Extrusion is the most widely employed technique to the preparation of porous ceramic tubes for the use as the separation membrane or the support of chemically recognizable or reactive membranes.[9–11] Unlike the polymer melts, the blend of a polymer melt and a ceramic powder with high volume fraction (e.g. 80–85 wt.%) requires a much larger extrusion pressure. The polymer melt in the blend behaves very differently from itself alone in response to the applied shear stress. Nevertheless, the past experience of the polymer–ceramic interactions came primarily from the blends with low solid contents.[12,13]

One of the most popular mathematical models describing the dependence of the shear stress on the shear rate of the blend is the Herschel–Bulkley (HB) model:[14,15]

$$\tau = \tau_0 + K\dot{\gamma}^m \quad (1)$$

in which τ is the applied stress, τ_0 the yield stress accounting for the interactions of polymer and polymer, polymer and particle, and particle and particle under very low shear rate $\dot{\gamma}$; K is the consistency modulus, and the index m stands for the effect of high share rates. For Bingham plastic flow, m equals

* Corresponding author. Tel.: +65 6874 5029; fax: +65 6779 1936.
E-mail address: chehongl@nus.edu.sg (L. Hong).

0955-2219/$ – see front matter © 2004 Elsevier Ltd. All rights reserved.
doi:10.1016/j.jeurceramsoc.2004.09.018

to unity.[16] Similarly, several other mathematical models have been developed to describe the relationship between the relative viscosity (η_{rel}) of the blend and the solid powder content expressed by volume fraction (ϕ). The most feted one should be regarded as the theoretical Einstein model:[16]

$$\eta_{rel} = 1 + 2.5\phi \tag{2a}$$

Einstein relationship is valid only for very low solid loading systems ($\phi \ll 1$) and requires the solid particles to be spherical with an identical radius.

Several empirical or semi-empirical formula have been developed thus far to describe the relationship $\eta_{rel} \sim \phi$, such as power series (Eq. (2b)), Eilers' equation (Eq. (2c)), Mooney model (Eq. (2d))[17] and Krieger–Dougherty model[15,16,18,19] (Eq. (2e)). These models can be viewed as the modified forms of the Einstein's equation by adjusting the contribution of ϕ to η_{rel}. In spite of this, these models do not justify the variations of the influence of ϕ on the defining physical chemistry basis:

$$\eta_{rel} = 1 + 2.5\phi + \sum_{n=2} A_n \phi^n \tag{2b}$$

$$\eta_{rel} = \left(1 + \frac{2.5\phi}{1 - (\phi/\phi_{max})}\right)^2 \tag{2c}$$

$$\eta_{rel} = \exp\left(\frac{2.5\phi}{1 - (\phi/\phi_{max})}\right) \tag{2d}$$

$$\eta_{rel} = \left(1 - \frac{\phi}{\phi_{max}}\right)^{K\phi_{max}} \approx \left(1 - \frac{\phi}{\phi_{max}}\right)^{-2.5\phi_{max}} \tag{2e}$$

To endow the hard spheres certain sorts of surface characteristics (such as the adsorbed species), the effective solid loading (ϕ_{eff}) has been used in place of ϕ in the above equations (Eq. (3)):

$$\phi_{eff} = \phi\left(1 + \frac{\delta}{R}\right) \tag{3}$$

where δ is the thickness of the average adsorbate layer and R is the radius of the spherical adsorbent particles.

It is generally thought that interactions between polymers and ceramic particles are the root-cause of special rheological behavior that the blend possesses, and the interactions will become more significant with increasing the volume fraction of the ceramic phase in the blend. There are basically three factors governing the interactions happening at the polymer–ceramic phase boundary: firstly, the surface area of the ceramic particles available for adsorption, particularly, for the same ceramic content, the smaller the particles the higher will be the polymer–particle interface, and therefore more viscous will be the blend;[17,20,21] secondly, affinity of functional groups on the polymer backbone with the surface of ceramic particles or vice versa; this normally entails quasi-chemical bonding (e.g. Lewis acid–base pair) that drives the adsorption of polymer chains on ceramic particles; and thirdly, the flexibility of polymer backbone as well as the molecular weight distribution of polymer. A polymer chain with less steric hindrance to the chain motions would have higher probabilities to form multi-adsorption sites on different ceramic particles in the blend.

Besides the polymer–ceramic interactions, attractions between ceramic particles also exist in the blend, among which van der Waals (vdw) attractive forces play the main role; other types of forces, such as electrostatic attraction or repulsion may happen depending upon the surface charge levels. The entropic depletion force which is essentially the vdw force counts on the polydispersity of the ceramic particles in the blend. Understanding how theses forces act in the nanoparticle systems has become a recent research focus.[22] The vdw force is an ubiquitous force, which is generally responsible for the agglomeration of the particles and the particle–polymer separation,[23] whereas the electrostatic repulsion force is widely utilized to increase the stability of the dispersion of particles in a polymer medium.[24–27] On the other hand, through use of a pertinent polymer, particle aggregations can be prevented by virtue of the steric repulsion of the polymer chains adsorbed on ceramic particles.[28]

In a polymer–solid particle blend wherein if non-adsorption occurs, the polymer chains are likely to be pushed away from the space between any two particles due to the inter-particle attractions mentioned earlier. This exclusion of polymer molecules from the region leads to local agglomeration of the solid particles, and will be ending up with phase separation in the blend if "dislike" between polymer and particle determines the blend.[29–36] In reality, adsorptions of polymers on various ceramic particles happens in major polymer–particle blends as long as the polymer chains bear organic functional groups, and what matters is the adsorption strength versus temperature, which affects the rheological behaviors of a blend. In this context, studies on the rheological behaviors of the blend can retrospectively help gaining an insight into the polymer–particle interactions.

With respect to the preparation of a polymer–ceramic blend for extrusion or molding purpose, there are several approaches: (1) introduction of the desired ceramic powder into a polymer solution (followed by removing the solvent)[37–42] or into a polymer melt;[43] (2) use of organometallic polymers as pre-ceramic matrix;[44–49] and (3) perpetrating polymerization at the surface of ceramic fine particles.[50–53] Of these methods, direct solution mixing is obviously a simple and practical way to the preparation of extrusion feedstock.

This work prepared the polymer–ceramic blend comprising cerium oxide fine powders and polyethylene glycol (PEG) melt as a model system to study the dependence of relative viscosity of the blend on volume fraction of CeO_2 by a mathematical model. The experimental data obtained from measuring viscosity at low shear rates were employed to verify the model. This mathematic model includes the two fundamental interactions which are adsorption and vdw attraction as addressed earlier. PEG has a low and sharp melting point, surfactant-like property and ease of being burned out, these are also the merits of a desired polymer binder.[54]

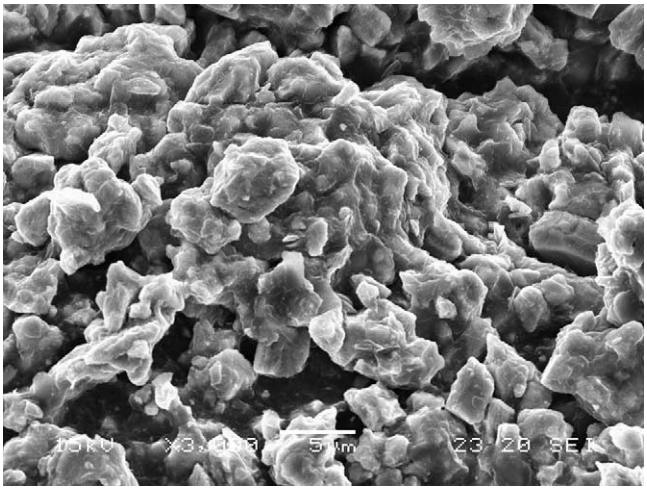

Fig. 1. Scanning electron micrographs of PEG–CeO_2 blend with 50 vol.% of CeO_2.

2. Experimental

2.1. Chemicals

Cerium(IV) oxide (CeO_2) powder was purchased from Strem Chemicals (CAS# 1306-38-3). The powder has the average particle size of about 4.8 μm (Fig. 1) and the bulk density of 7.3. Polyethylene glycol ($M = 15{,}000$) (Merck–Schuchardt), PEG-400 (Nacalai Tesque Inc.) and Tween® 80 (Aldrich) were used as binder, plasticizer and lubricant, respectively. All the above chemicals were used as received.

2.2. Preparation of CeO_2–PEG blend

At room temperature, CeO_2 powder was dispersed in an aqueous solution of PEG-400 and Tween® 80 (polyoxyethylene-20 sorbitan monolaurate) under continuous magnetic stirring (∼600 rpm). After mixing for 20 min, the resulting suspension was added into an aqueous solution of PEG-15,000 (20 wt.%) at room temperature. After mixing for 4 h, the slurry was subjected to evaporation at 80 °C till when the magnetic stirring became stuck. The concentrated slurry turned was manually blended while it was cooled down to room temperature. The remaining wet PEG–CeO_2 solid was dried under vacuum for at least 72 h at room temperature to obtain the desired blend for rhelogical study. Several PEG–CeO_2 compositions were formulated by varying the content of CeO_2, which are listed in Table 1. The rheological study (shear stress versus shear rate) was carried out by examining only the blends without containing the surfactant Tween® 80.

2.3. Rhelogical investigation

Measurements of the steady-state viscosity were performed by using a Brookfield viscometer (Brookfield DV-II).

Table 1
Composition of the CeO_2—polymer composites

Chemical	Function	Content[a]
CeO_2	Ceramic powder	1–80 wt.% (0.18–41.6 vol.%)
PEG-400	Plasticizer	5 wt.% of CeO_2
PEG-15,000	Binder	Variable
Tween® 80	Lubricant	Variable

[a] The mass densities of CeO_2 ($\rho = 7.3$) and PEG ($\rho = 1.3$) were used to compute vol.% of CeO_2.

A PEG–CeO_2 solid was loaded in a tubular aluminum sample holder, which was then placed in the accessory micro-oven. The measurement was conducted at temperatures above the melting point of PEG.

2.4. Differential scanning calorimetry (DSC) studies

DSC analysis of the PEG–CeO_2 blends was performed on the METTLER TOLEDO STAR DSC-821 scanning calorimeter in the temperature range from 25 to 100 °C. The measurement procedure included heating the sample to 100 °C (at the rate of 10 °C/min), and subsequently cooling it down to 25 °C (at the rate of −10 °C/min) to ensure all the samples under investigation have the same thermal history. The DSC data (T_g and T_m) were collected from the second scanning.

2.5. Other instrumental characterizations

X-ray diffraction (XRD) analysis was employed to examine the crystallization behavior of PEG. The analysis was carried out on a SHIMADZU XRD-6000 diffraction meter using Cu Kα radiation (λ = 1.54056 Å) and the scanning speed of 2.5°/min. The scanning angle was set from 10° and 60°. The adsorption of PEG on CeO_2 was identified by the infrared spectra of PEG obtained from a Bio-Rad FTIR FTS135 spectrometer. For this characterization, only PEG (15,000) was employed to form the blend with CeO_2. The morphology of the PEG–CeO_2 blend was observed on a scanning electron microscopy (SEM) instrument (JEOL JSM-5600).

3. Results and discussion

3.1. Adsorption and van der Waals attractive forces in CeO_2–PEG blend

When the content of CeO_2 powder in the blend was raised to the comparable or higher level than that of PEG phase, the PEG phase becomes a jacket of CeO_2 particles (Fig. 1). This phenomenon shows that PEG wets CeO_2 surface well and hence a thorough mixing of both achieves readily. Likewise, XRD (Fig. 2a) characterization proved that the crystallinity of PEG phase dropped drastically even at a rather low volume fraction of CeO_2, i.e. $\phi = 7.1$ vol.% (or 26.8 wt.%). It could be ascribed to the strong adsorption tendency of PEG

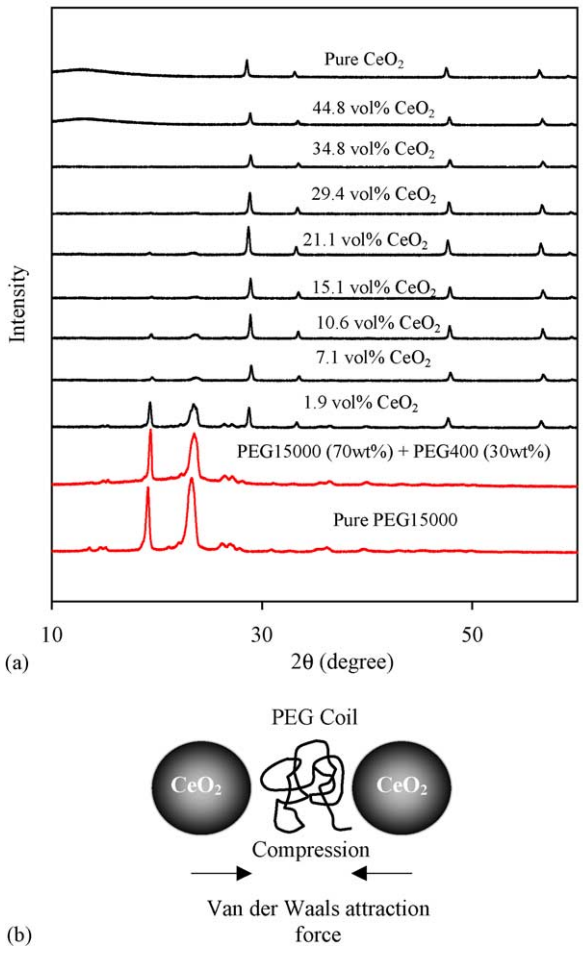

Fig. 2. XRD of the PEG–CeO_2 blends with different CeO_2 loadings. A schematic illustration to show compressive effect on PEG coils due to instant inter-particle attraction.

segments onto CeO_2 particles, namely the orderly folding of PEG chains (crystallization) became impossible in the adsorption layer.

From the SEM image (Fig. 1), the rifts between particles were smaller than the sizes of CeO_2 particles. With this aspect ratio, the vdw attractive forces between CeO_2 particles became inevitable. As far as this type of surface–surface interaction is concerned, Myers[55] used an ideal model to describe the situation: two identical spheres of radius R are separated in vacuum by a distance H, when $H/R \ll 1$, the free energy of attraction per unit area is approximated by:

$$\Delta G^{\text{att}} = -\left(\frac{A_{\text{H}}R}{12H}\right)\left[1 + \frac{3}{4}\frac{H}{R} + \text{higher terms}\right] \quad (4a)$$

where $A_{\text{H}} = (3/4)h\nu\alpha_0^2\pi^2N^2$ is the Hamaker constant in vacuum (α_0 is the electronic polarizability of the atoms, $h\nu$ is related to the first ionization potential of the atoms, and N is the number of atoms in unit volume of the spheres.) When the two particles (surface) are separated by a medium, $A_{\text{H}}^{\text{eff}}$ is used in lieu of A_{H} to approximate such a more complex system, where $A_{\text{H}}^{\text{eff}}$ takes the mathematic form including the

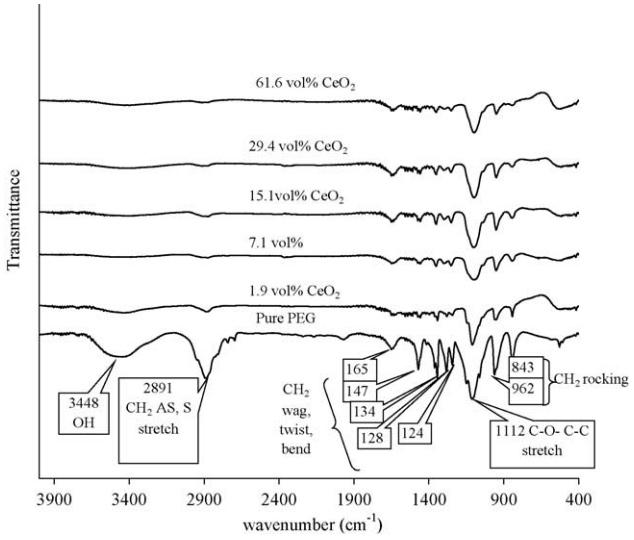

Fig. 3. FT-IR spectra of PEG–CeO_2 blends with different CeO_2 loadings.

Hamaker constants of the two phases. Despite the fact that Eq. (4a) could describe far from precisely the free energy existing between CeO_2 particles in the blend due to geometric and compositional irregularities, it still does not lose the sense of being the ground for studying real systems. The free energy of inter-particle attraction is a crucial factor affecting the rheological responses of the composition with high CeO_2 loadings (ϕ) to shear stress.

The inter-particle attraction is considered to generate compressive force on the PEG chains (Fig. 2b). FT-IR spectra of the PEG–CeO_2 mixtures furnish the evidence to this theoretical inference (Fig. 3). The useful information from the IR analysis is the vibration absorption band of the C–O–C bond at 1112 cm^{-1}; this band became blunt when the CeO_2 loading reached 7.1 vol.% from 1.9 vol.%, and after that, the band resumed somewhat its original shape with the increasing of CeO_2 content. This phenomenon can be understood by both the effects of inter-particle attraction and adsorption of PEG on CeO_2. Under the compression of CeO_2 particles, the bond angle of C–O–C of PEG segments would engage a certain extent of deformation, which caused changes in its stretching modulus and therefore in the shape of C–O–C IR absorption band. Although the compression on PEG became more severe with increasing ϕ of CeO_2 particles, the PEG molecules adsorbed on CeO_2 particles, on the other hand, countered the deformation of bond angles due to the "fixation" effect. The number of adsorbed PEG molecules increased with increasing CeO_2 loading in the blend, and as a result, the IR band of C–O–C vibration reflected the molecular conformation of this portion of molecules, which look more like free PEG molecules.

In addition to the XRD investigation, coherent message about structural changes of the PEG phase due to adsorption on CeO_2 particles can also be acquired from the DSC analysis. The two blends composed of 41.6 vol.% CeO_2 and the PEG phase (consisting of PEG-15,000 and PEG-400) were

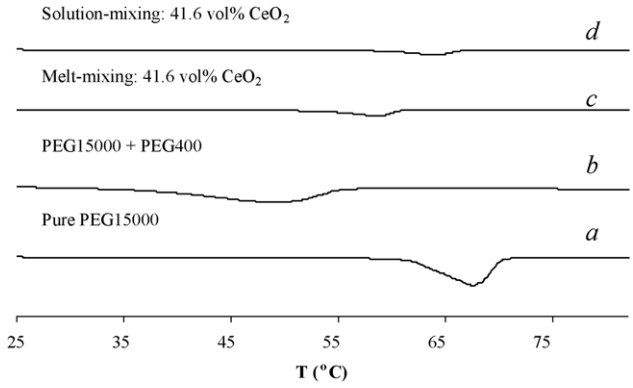

Fig. 4. DSC profiles of: (a) pure PEG-15,000; (b) mixture of PEG-15,000 (80 vol.%) and PEG-400 (20 vol.%); (c) mixture of PEG-15,000 (46.72 vol.%), PEG-400 (11.68 vol.%) and CeO_2 (41.6 vol.%) made by melt mixing method; (d) the same as (c) but made by solution mixing method.

employed as the typical samples to exhibit the occurrence of strong physical adsorption (Fig. 4). Compared with the single PEG phase (a mixture of PEG-15,000 and PEG-400), the PEG phase in both blends displayed higher glass transition temperatures. It was an indication that the adsorption "bonding" restricted segment motions, e.g. rotations and creeps of PEG macromolecules, as what the "fixation" refers to in the above section. Moreover, the two different preparation procedures (solution versus fusion) also gave rise to different thermal response of the PEG phase, which revealed that the solution blending procedure resulted in a more thorough mixing blend because of higher T_g, which is ascribed to the existence of a higher PEG–CeO_2 interface in the blend.

3.2. Relative viscosity of the PEG–CeO_2 blend

The shear stress (σ)–strain rate ($\dot{\gamma}$) relationship of the melts of PEG–CeO_2 blends with different ϕ of CeO_2 all displayed Bingham fluid behavior within the low shear stress range at various temperatures (Fig. 5a–c). With respect to temperature effect, the sample containing 21.1 vol.% of CeO_2 showed a steady reduction of viscosity with raising temperature (Fig. 5a). With respect to the effect of CeO_2 loading at a fixed temperature, the higher the CeO_2 content the greater the viscosity was observed as expected; for this study two temperature points (140 and 160 °C) were examined (Fig. 5b and c). It is worthy to note that the viscosity of the blend containing 41.6 vol.% of CeO_2 became somewhat smaller than that of the blend with 21.1 vol.% of CeO_2 at 160 °C. This apparent drop in shear stress caused by raising temperature from 140 to 160 °C is deemed as the squeezing effect due to presence of the vdw attractive forces among CeO_2 particles. At 160 °C, the PEO phase became easier to free from interparticle spaces in the blend with the higher CeO_2 content under the compression as quoted earlier. In other words, the

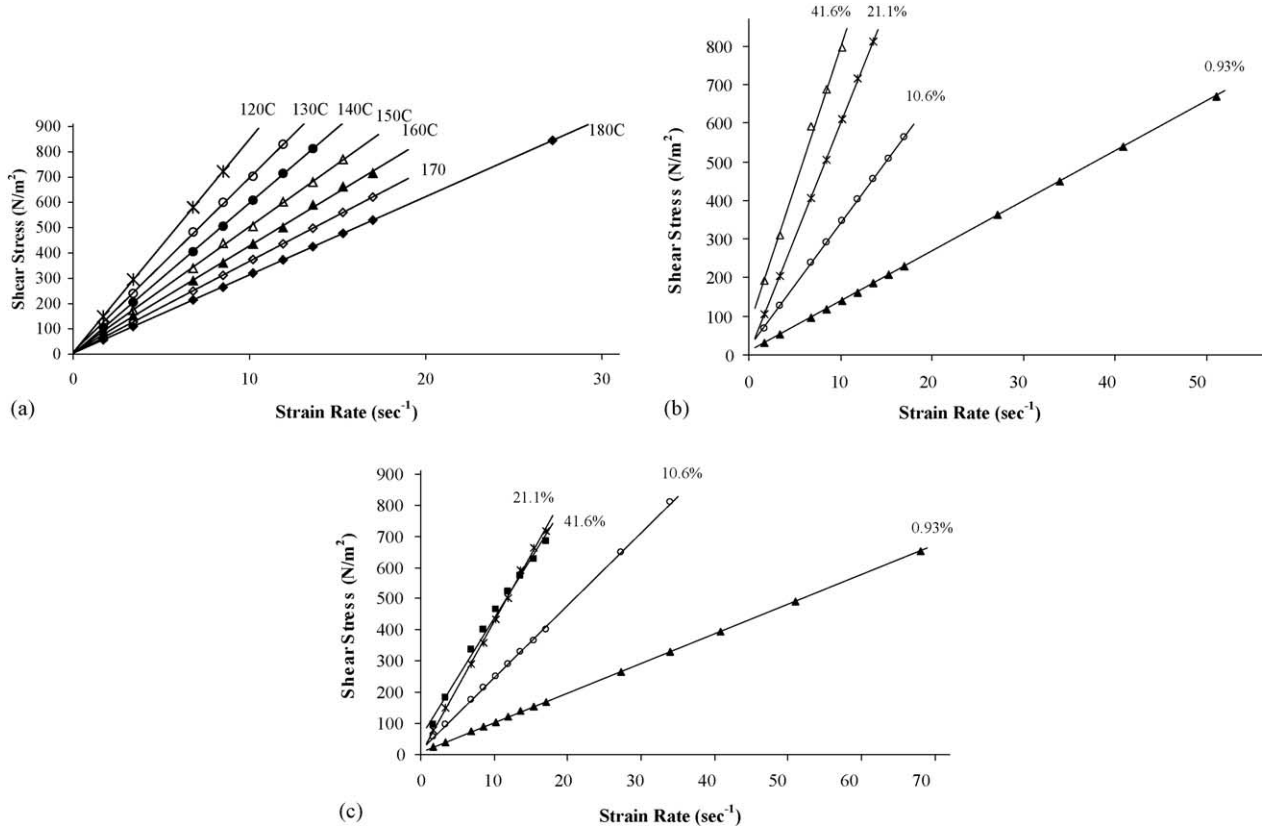

Fig. 5. (a) Dependence of shear stress (σ) on shear rate ($\dot{\gamma}$) at different temperatures using the blend containing 21.1 vol.% of CeO_2 as the model. (b) The investigation in the effect of CeO_2 loading on $\sigma \sim \dot{\gamma}$ response at 140 °C. (c) The investigation in the effect of CeO_2 loading on $\sigma \sim \dot{\gamma}$ response at 160 °C.

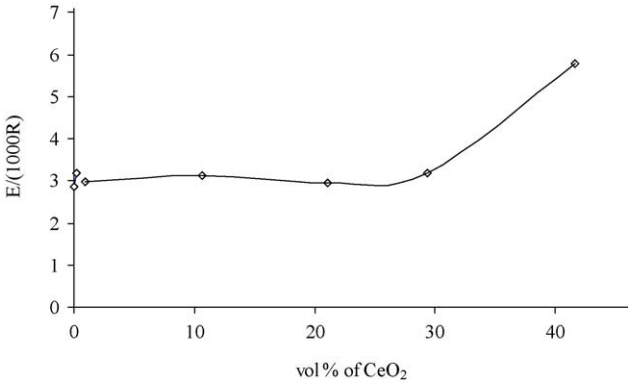

Fig. 6. Dependence of the activation energy of viscous flow on the volume fraction of CeO_2.

partial phase separation caused by raising temperature lowered down the activation energy of viscous flow. The trend revealed in this study represents a common fact: the mixing extent between a ceramic powder and a polymer phase decreases with increasing the ceramic content.

The temperature dependence of apparent viscosity of the blend melt obeyed satisfactorily the Arrhenius relation (obtained based on seven or eight temperature points in the range of 100–180 °C). The activation energy barrier of viscous flow did not vary noticeably with the CeO_2 loadings below roughly 25 vol.% (Fig. 6), which meant that there was a slippery PEG layer between CeO_2 particles before this ϕ value. A sensible explanation would be the adsorption of PEG on CeO_2 particles, which induced free volumes surrounding particles through irregular screwing up of PEG chains (Fig. 7a). The further climbing up of the activation energy symbolized formation of a physical network (Fig. 7b), in which the CeO_2 particles behaved as cross-linking points to make the viscous flow take place collectively.

A mathematical model is established to express the rheological behavior of the PEG (melt)–CeO_2 blend. The volume fraction of ceramic particles (ϕ) could be expressed by a simple mathematic formula that assumes the ceramic particles be hard spheres with identical radius of R and stacked with simple cubic structure:

$$\phi = \frac{(4/3)\pi}{(2+L)^3} \tag{4b}$$

However, since CeO_2 particles have irregular shapes and are polydispersed, to satisfy the model, these irregular particles can be equivalent to a certain number of spheres with radius R on the basis of unchanged in the surface area. As noted earlier, the H value is the boundary distance between two adjacent balls, $L = H/R$ is a dimensionless quantity signifying effective distance for vdw attractive forces. Eq. (4b) can thus be rewritten as:

$$L = \left(\frac{4\pi}{3\phi}\right)^{1/3} - 2 \tag{4c}$$

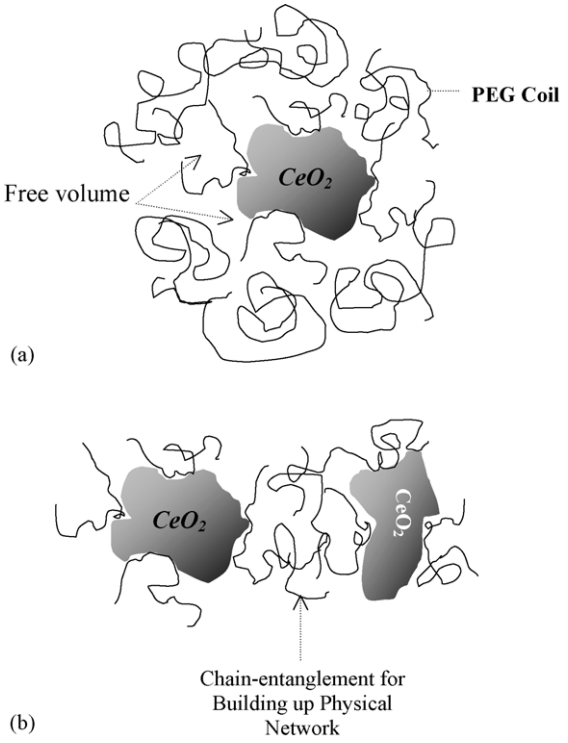

Fig. 7. (a) A schematic illustration of the generation of free volume at the interfacial boundary between PEG and CeO_2 particles. (b) A schematic illustration of the formation of the physical network due to adsorption.

If ϕ is sufficiently low so as the inter-particle attraction can be neglected, the influence of the particles on rheology of the blend is thus mainly determined by the free volumes generated near the surface of individual particles as depicted in Fig. 7a. The Arrhenius equation was considered as a pertinent and succinct theoretical model[55] to describe the particle effect on viscosity. Equivalently, this concept is applied hereby to express the relative viscosity η_{rel} of the PEG–CeO_2 blend:

$$\eta_{rel} = \frac{\eta}{\eta_0} = \frac{k\ \exp(E/RT)}{k_0\ \exp(E^0/RT)} = K\ \exp\left(\frac{\Delta E}{RT}\right) \tag{5}$$

where E^0 is the energy barrier to the flow of Bingham plastic of the single PEG melt (comprising PEG-15,000 and PEG-400), E is the energy barrier to the Bingham flow of the PEG (melt)–CeO_2 blend, k, k_0, and K are constants. Therefore, ΔE reflects the contributions of polymer–particle interaction (ΔE^{ad}) and particle–particle interactions (ΔE^{vdw}) at a given temperature.

It is known that Einstein equation (Eq. (2a)) describes the hydrodynamic effect of the monodispersed hard spherical particles possessing a low volume fraction in a continuous medium. Since the CeO_2 particles used in the present real system are neither spherical ball nor monodispersed, the Einstein equation has to be modified by redefining its second terms:

$$\eta_{rel}^{ad} = 1 + B\phi \tag{6}$$

where B is the parameter including the effect of the surface area of CeO_2 particles which are the absorbent of PEG segments and therefore the cross-linking point of the physical networks formed. The physical cross-linking gives rise to a strong hydrodynamic drag on the flow of PEG melt (Fig. 7b). Moreover, B value also embraces the influences of irregular shape and different sizes of the CeO_2 particles on the viscosity. The superscript "ad" symbolizes the contribution of adsorption to the elastic component of the flow.

In the high-particle-loading blend, the vdw attractive forces act in the same way as the cross-adsorbed PEG chains to strengthen the network (or elastic) property of the blend, and then to impede the flow of PEG melt. From this perspective, the activation energy of viscous flow of the PEG melt (ΔE) can be correlated with the vdw attraction. Hamaker model[26,27] describes the vdw potential (ζ) between two particles by the simple form:

$$\zeta = -\frac{A_0}{L^n} \tag{7a}$$

in which A_0 and L have been defined before, n is the parameter determined by the shape of particles:

$$\Delta E^{\mathrm{vdw}} = -k'\zeta = \frac{k'A_0}{L^n} = \frac{A}{L^n} \tag{7b}$$

Table 2
Parameter values of different models under different temperature

Model	Parameter	140 °C	150 °C	160 °C
Eilers	ϕ_m	0.75	0.84	0.97
Modified Eilers	k	3.26	2.93	2.64
	ϕ_m	1	1	1
Mooney	ϕ_m	0.73	0.78	0.84
Modified Mooney	k	3.40	3.18	2.97
	ϕ_m	1	1	1
Krieger–Dougherty	ϕ_m	0.48	0.50	0.53
Modified Krieger–Dougherty	k	4.49	4.21	3.93
	ϕ_m	1	1	1
Our model ($n=1$)	A	15.93	11.69	4.88
	B	14.90	14.51	14.49
Our model ($n=2$)	A	111.27	85.60	39.98
	B	12.86	13.10	13.92

The contribution of the particle–particle attraction component to retarding the viscous flow can be approximated by the linear relation between ΔE^{vdw} and ζ, k' is the proportional constant and also has the significance of the number of particle–particle pairs per unit volume. Combination of equations (4c), (5) and (7b) enables the vdw attraction to be mathematically related to the relative viscosity for the high

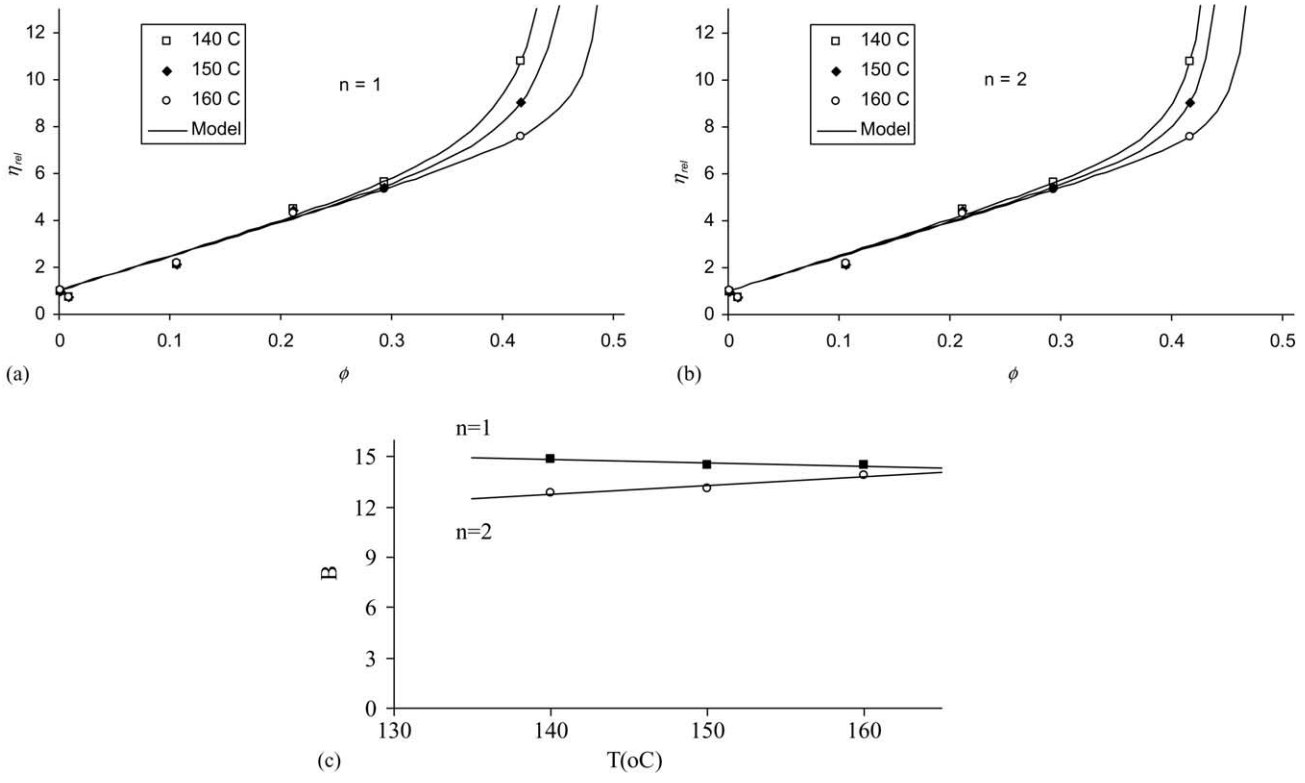

Fig. 8. Demonstration of the fitting results of the model developed to the experimental $\eta_{rel} \sim \phi$ data at different temperatures: (a) the model assuming spherical CeO_2 particle shape ($n=1$); (b) the model assuming rod-like CeO_2 particle shape ($n=2$); (c) dependence of the simulated parameter value B on temperature.

CeO_2-loading blend:

$$\eta_{\mathrm{rel}}^{\mathrm{vdw}} = \exp\left\{\frac{A}{[(4\pi/3\phi)^{1/3} - 2]^n RT}\right\} \quad (8)$$

Consequently, the total relative viscosity (η_{rel}) of the blend should include both $\eta_{\mathrm{rel}}^{\mathrm{vdw}}$ (Eq. (8)) and $\eta_{\mathrm{rel}}^{\mathrm{ad}}$ (Eq. (6)) terms, which are corresponding to ΔE^{vdw} and ΔE^{ad}, respectively:

$$\eta_{\mathrm{rel}} = \eta_{\mathrm{rel}}^{\mathrm{ad}} + \eta_{\mathrm{rel}}^{\mathrm{vdw}} \cong \exp\left\{\frac{A}{\left[(4\pi/3\phi)^{1/3} - 2\right]^n RT}\right\} + B\phi \quad (9)$$

Fitting the model with experimental data ($\eta_{\mathrm{rel}} \sim \phi$ at an assigned T and n) by using the linear least square method, we were able to determine the numerical values of A and B (Table 2). The fitted value of B is much higher than the corresponding parameter in the Einstein equation (Eq. (2a)). In contrast to the original Einstein model that considers only the mechanical resistance of individual hard spheres to the flow of the continuous fluid ($\eta_{\mathrm{rel}} = 1 + 2.5cV_{\mathrm{ball}}$), where c is the number of spherical balls per unit volume and V_{ball} the volume of a single sphere), the B value obtained from the simulation reflects the real resistance to the viscous flow due to the adsorption of a polymer layer on particles as well as the formation of the physical network. Values B determined at the three different temperatures (140, 150 and 160 °C) were rather similar. This outcome is indicative of a sluggish desorption of PEG from CeO_2 particles with increasing temperature in the range of study. On the other hand, value A decreased sharply with increasing temperature, which suggests that the vdw attractive forces in the blend with a high ϕ are susceptible to temperature, in connection this conclusion with the preceding interpretation to the $\sigma \sim \dot{\gamma}$ response of the blend with $\phi = 41.6\%$ (in Fig. 5c), it is likely that agglomeration of CeO_2 particles due to loss of the PEO layer separating them is the reason for the reduction of A values.

Fig. 8 shows the experimental data and the simulated curves based on Eq. (9). This model fits well the experimental data. In comparison with the other three well-known models, they depart away from the experimental data more noticeably (Fig. 9). Table 2 lists numerical values of the parameters of these three models, which were obtained from simulating the experimental data. Each model had both single and double parameter forms; the latter one came from replacing the number of 2.5 with the parameter k, which was introduced as the crowding factor. This substitution led to the modified (or two-parameter) Eilers (Eq. (10a)),[55] Mooney (Eq. (10b))[17] and Krieger–Dougherty models (Eq. (10c)),[19,56,57] respectively:

$$\eta_{\mathrm{rel}} = \left(1 + \frac{k\phi}{1 - (\phi/\phi_{\max})}\right)^2 \quad (10a)$$

$$\eta_{\mathrm{rel}} = \exp\left(\frac{k\phi}{1 - (\phi/\phi_{\max})}\right) \quad (10b)$$

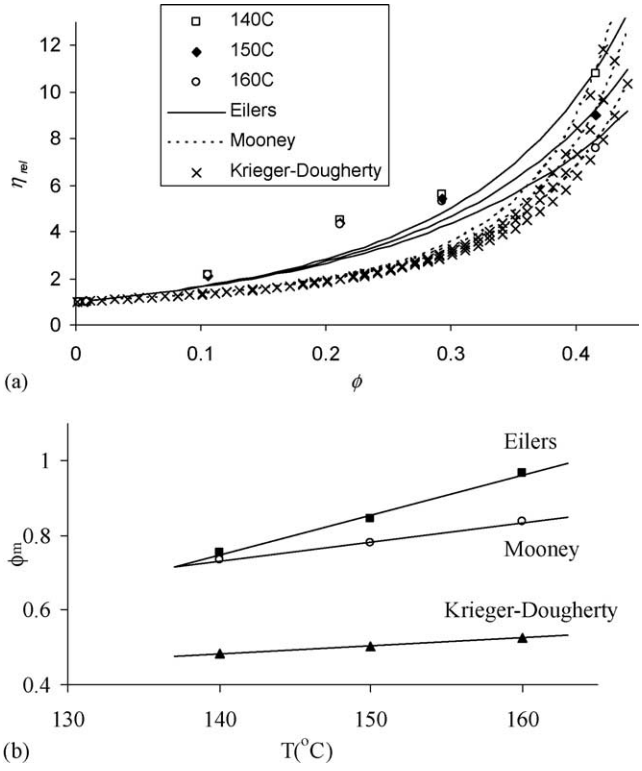

Fig. 9. (a) Comparison of the fitting results of the three common models with the experimental $\eta_{\mathrm{rel}} \sim \phi$ data at different temperatures. (b) Dependence of simulated parameter ϕ_m value on temperature.

$$\eta_{\mathrm{rel}} = \left(1 - \frac{\phi}{\phi_{\max}}\right)^{-k\phi_{\max}} \quad (10c)$$

The modified models fit the experimental data slightly better (Fig. 10) than their corresponding unmodified models in the range of $0 < \phi_{\max} \leq 1$. In conclusion, the model described by Eq. (9) portrays more closely the real roles of CeO_2 particles in affecting the viscous flow of PEG melt in the blend. The roles are divided as two respects: the vdw attractive forces among CeO_2 particles and the physical network that is contingent upon the adsorption of PEO segments on CeO_2 particles.

3.3. Surfactant effect

Non-ionic surfactants bearing hydrophilic polyoxyethylene oligomer blocks have often been used as the deflocculation reagent for fine ceramic oxide powders.[58] This particular functionality is attributed to the adsorption of the hydrophilic moiety on the metal-oxide particles through the Lewis acid–base interaction or hydrogen bonding. In this way, the surfactant molecules would form one or more adsorption layers on oxide particles (Fig. 11) depending upon the amount of surfactant used. Tween® 80 was employed in this work as the plasticizer for the PEG–CeO_2 (41.6 vol.%) blend to reduce its low temperature extrusion viscosity. The viscous flow activation energy of the blend decreased quickly

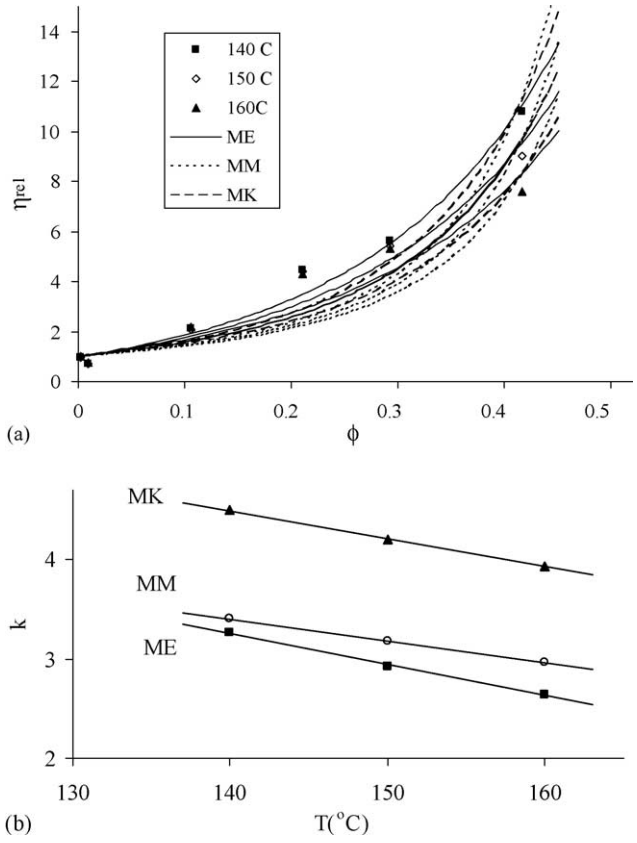

Fig. 10. (a) Comparison of the fitting results of the modified Eilers (ME) model, Mooney (MM) model and Krieger–Dougherty (MK) model with the experimental $\eta_{rel} \sim \phi$ data at different temperatures. (b) Dependence of simulated parameter k value on temperature.

before 2 wt.% and level off after that (Fig. 12). This phenomenon can be understood from the multi-adsorption structure laid out in Fig. 11, firstly, the hydrophobic block of Tween® 80 leads to a hydrophobic slippery layer, which is responsible for the decrease of melt viscosity; secondly, only the most inner slippery layers play the primary role in lubricating the flow of PEG melt as these hydrophobic layers feel the greatest torque.

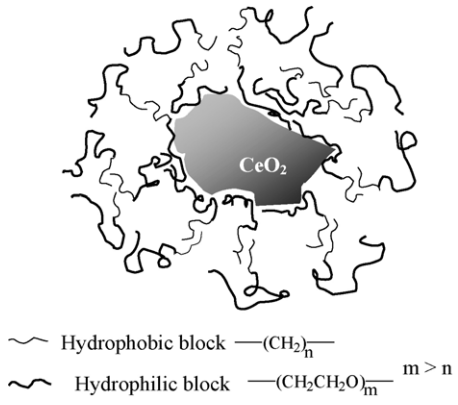

Fig. 11. A schematic illustration of the multi-layer adsorption of Tween® 80 molecules on CeO_2 particles.

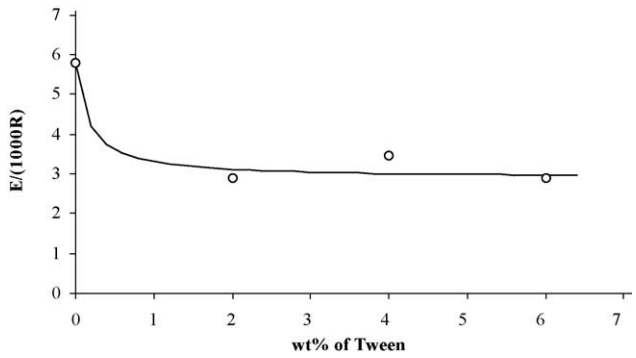

Fig. 12. Lubricating effect of Tween® 80 on the viscous flow of PEG–CeO_2 (41.6 vol.%) blend.

4. Conclusions

The PEG–CeO_2 blends prepared via mixing CeO_2 fine powder with an aqueous solution of PEG and then removing water is an appropriate system, because of the thorough mixing extent, for the study of particle effects on viscous flow of the PEG melt under low shear rates. The XRD and DSC analyses of the resultant blends differentiated by the loading of CeO_2 (ϕ in vol.%) proved occurrence of strong adsorption of PEG chains on CeO_2 particles. The adsorption led to formation of a physical cross-linking network, especially in the high CeO_2-loading blends. On the other hand, the characteristic infrared absorption band of the PEG (ν_{C-O-C}) undergo changes in both frequency and intensity with increasing ϕ value, which was ascribed to the existence of interparticle van der Waals attractive forces among CeO_2 particles. These two fundamental interactions (adsorption and vdw attraction) are considered as the prevalent forces in such a polymer–ceramic blending system. A mathematic model expressing the relative viscosity (η_{rel}) as the function of ϕ, T, and the geometry/surface states of CeO_2 particles (n/B) was established on the basis of the Einstein equation and the Arrhenius relationship. In this mathematic model, the activation energy of viscous flow consists of two parts, the barrier due to formation of the physical cross-linking network ($\Delta E^{ad} \sim \eta_{rel}^{ad}$) and the barrier due to the presence of vdw attractive forces ($\Delta E^{vdw} \sim \eta_{rel}^{vdw}$). In parallel, under the low shear rates, the blends display Bingham flow behavior with respect to a series of ϕ at temperatures above the melting point of PEG. This mathematic model could more precisely match the experimental $\eta_{rel} \sim \phi$ data within the designated range of shear rates and temperatures by comparing with the three commonly used models. An additional study was also carried out to understand non-ionic surfactant effect on lowering down the melt viscosity of the blends. The concept of slippery hydrophobic shell is proposed to explain the fact that there is a lowest critical concentration of surfactant.

References

1. Guizard, C., Ayral, A. and Julbe, A., Potentiality of organic solvents filtration with ceramic membranes. A comparison with polymer membranes. *Desalination*, 2002, **147**(1–3), 275–280.
2. Xu, L., Li, W., Lu, S., Wang, Z., Zhu, Q. and Ling, Y., Treating dyeing waste water by ceramic membrane in crossflow microfiltration. *Desalination*, 2002, **149**(1–3), 199–203.
3. Gan, Q., Howell, J. A., Field, R. W., England, R., Bird, M. R., O'Shaughnessy, C. L. *et al.*, Beer clarification by microfiltration—product quality control and fractionation of particles and macromolecules. *J. Membr. Sci.*, 2001, **194**(2), 185–196.
4. Kao, Y. K., Lei, L. and Lin, Y. S., Optimum operation of oxidative coupling of methane in porous ceramic membrane reactors. *Catal. Today*, 2003, **82**, 255–273.
5. Liu, Q.-L. and Li, Q.-B., Membrane of PVA coated on porous catalytic ceramic disks supported $H_3PW_{12}O_{40}$. *J. Membr. Sci.*, 2002, **202**(1–2), 89–95.
6. Julbe, A., Farrusseng, D. and Guizard, C., Porous ceramic membranes for catalytic reactors—overview and new ideas. *J. Membr. Sci.*, 2001, **181**(1), 3–20.
7. Ziegler, S., Theis, J. and Fritsch, D., Palladium modified porous polymeric membranes and their performance in selective hydrogenation of propyne. *J. Membr. Sci.*, 2001, **187**(1–2), 71–84.
8. Cot, L., Ayral, A., Durand, J., Guizard, C., Hovnanian, N., Julbe, A. *et al.*, Inorganic membranes and solid state sciences. *Solid State Sci.*, 2000, **2**, 313–314.
9. Kaya, C., Butler, E. G. and Lewis, M. H., Co-extrusion of Al_2O_3/ZrO_2 Bi-phase high temperature ceramics with fine scale aligned microstructures. *J. Eur. Ceram. Soc.*, 2003, **23**(6), 935–942.
10. Hurysz, K. M. and Cochran, J. K., The application of models for high solids content suspensions to pastes. *J. Eur. Ceram. Soc.*, 2003, **23**(12), 2047–2052.
11. Habelitz, S., Carl, G. and Rüssel, C., Processing, microstructure and mechanical properties of extruded mica glass-ceramics. *Mater. Sci. Eng. A*, 2001, **307**, 1–14.
12. Chen, Y., Burbidge, A. and Bridgwater, J., Effects of carbohydrate on the rheological parameters of paste extrusion. *J. Am. Ceram. Soc.*, 1997, **80**(7), 1841–1850.
13. Burbidge, A. S. and Bridgewater, J., The single screw extrusion of pastes. *Chem. Eng. Sci.*, 1995, **50**(16), 2531–2543.
14. Wight Jr., J. F. and Reed, J. S., Nonaqueous aluminum nitride extrusion. II. Die-land flow and tribology. *J. Am. Ceram. Soc.*, 2002, **85**(7), 1689–1694.
15. Rangarajan, S., Qi, G., Venkataraman, N., Safari, A. and Danforth, S. C., Powder processing, rheology, and mechanical properties of feedstock for fused deposition of Si_3N_4 ceramics. *J. Am. Ceram. Soc.*, 2000, **83**(7), 1663–1669.
16. Lewis, J. A., Colloidal processing of ceramics. *J. Am. Ceram. Soc.*, 2000, **83**(10), 2341–2359.
17. (a) Mooney, M., The viscosity of a concentrated suspension of spherical particles. *J. Colloid Sci.*, 1951, 6–162;
    (b) Guyot, A., Chu, F., Schneider, M., Graillat, C. and McKenna, T. F., High solid content latexes. *Prog. Polym. Sci.*, 2002, **27**(8), 1573–1615.
18. Bergström, L. and Sjöström, E., Temperature induced gelation of concentrated ceramic suspensions: rheological properties. *J. Eur. Ceram. Soc.*, 1999, **19**(12), 2117–2123.
19. (a) Krieger, I. M. and Dougherty, T. J., Concentration dependence of the viscosity of suspensions. *Trans. Soc. Rheol.*, 1959, 3–137;
    (b) Quemada, D. and Berli, C., Energy of interaction in colloids and its implications in rheological modeling. *Adv. Colloid Interface Sci.*, 2002, **98**(1), 51–85.
20. Spalla, O., Nanoparticle interactions with polymers and polyelectrolytes. *Curr. Opin. Colloid Interface Sci.*, 2002, **7**, 179–185.
21. Steward, P. A., Hearn, J. and Wilkinson, M. C., An overview of polymer latex film formation and properties. *Adv. Colloid Interface Sci.*, 2000, **86**(3), 195–267.
22. Rao, C. N. R. and Cheetham, A. K., Science and technology of nanomaterials: current status and future prospects. *J. Mater. Chem.*, 2001, **11**(12), 2887–2894.
23. Goodwin, J. W. and Hughes, R. W., The dynamics and phase of concentrated dispersions. *Adv. Colloid Interface Sci.*, 1992, **42**, 303–351.
24. Giesbers, M., Kleijn, J. M. and Stuart, M. A. C., The electrical double layer on gold probed by electrokinetic and surface force measurements. *J. Colloid Interface Sci.*, 2002, **248**(1), 88–95.
25. Zhou, Z., Scales, P. J. and Boger, D. V., Chemical and physical control of the rheology of concentrated metal oxide suspensions. *Chem. Eng. Sci.*, 2001, **56**(9), 2901–2920.
26. Hsu, J.-P., Huang, S.-W., Kuo, Y.-C. and Tseng, S., Stability of a dispersion of particles covered by a charge-regulated membrane: effect of the sizes of charged species. *J. Colloid Interface Sci.*, 2003, **262**(1), 73–80.
27. Wennerström, H., The van der Waals interaction between colloidal particles and its molecular interpretation. *Colloids Surf. A: Physicochem. Eng. Aspects*, 2003, **228**, 189–195.
28. Tadros, T., Interaction forces between particles containing grafted or adsorbed polymer layers. *Adv. Colloid Interface Sci.*, 2003, **104**, 191–226.
29. Ye, X., Narayanan, T., Tong, P., Huang, J. S., Lin, M. Y., Carvalho, B. L. *et al.*, Depletion interactions in colloid–polymer mixtures. *Phys. Rev. E*, 1996, **54**(6), 6500–6510.
30. Lee, J. T. and Robert, M., Phase transitions of colloid–polymer systems in two dimensions. *Phys. Rev. E*, 1999, **60**(6), 7198–7202.
31. Moussaïd, A., Poon, W. C. K., Pusey, P. N. and Soliva, M. F., Structure of marginal and fully developed colloidal liquids. *Phys. Rev. Lett.*, 1999, **82**, 225–228.
32. Ilett, S. M., Orrock, A., Poon, W. C. K. and Pusey, P. N., Phase behavior of a model colloid–polymer mixture. *Phys. Rev. E*, 1995, **51**(2), 1344–1353.
33. Sear, R. P., Entropy-driven phase separation in mixtures of small colloidal particles and semidilute polymers. *Phys. Rev. E*, 1997, **56**(4), 4463–4466.
34. Sear, R. P., Phase separation in mixtures of colloids and long ideal polymer coils. *Phys. Rev. Lett.*, 2001, **86**(20), 4696–4699.
35. Tanaka, H., Viscoelastic model of phase separation. *Phys. Rev. E*, 1997, **56**(4), 4451–4462.
36. Verma, R., Crocker, J. C., Lubensky, T. C. and Yodh, A. G., Entropic colloidal interactions in concentrated DNA solutions. *Phys. Rev. Lett.*, 1998, **81**(18), 4004–4007.
37. Ford, J. V., Sumpter, B. G., Noid, D. W. and Barnes, M. D., Domain-size effects in optical diffraction from polymer/composite microparticles. *J. Phys. Chem. B*, 2000, **104**(3), 495–502.
38. Parvulescu, V., Buhoci, L., Roman, G., Albu, B. and Popescu, G., Composite membranes with micro- or mesoporous silicates and organic polymers. *Sep. Purif. Technol.*, 2001, **25**, 25–32.
39. Maiya, P. S., Picciolo, J. J. and Dusek, J. T., *Dense ceramic membrane material for conversion of methane to syngas*. US patent US6117808, 12 September 2000.
40. Croce, F., Curini, R., Martinelli, A., Persi, L., Ronci, F. and Scrosati, B., Physical and chemical properties of nanocomposite polymer electrolytes. *J. Phys. Chem. B*, 1999, **103**(48), 10632–10638.
41. Holland, B. T., Blanford, C. F. and Stein, A., Synthesis of macroporous minerals with highly ordered three-dimensional arrays of spheroidal voids. *Science*, 1998, **281**, 538–540.
42. Yoshida, W., Castro, R. P., Jou, J. D. and Cohen, Y., Multilayer alkoxysilane silylation of oxide surfaces. *Langmuir*, 2001, **17**(19), 5882–5888.
43. Zanetti, M., Kashiwagi, T., Falqui, L. and Camino, G., Cone calorimeter combustion and gasification studies of polymer layered silicate nanocomposites. *Chem. Mater.*, 2002, **14**(2), 881–887.

44. Corriu, R. J. P., Gerbier, P., Guérin, C. and Henner, B., From preceramic polymers with interpenetrating networks to SiC/MC nanocomposites. *Chem. Mater.*, 2000, **12**(3), 805–811.
45. Gabriel, A. O., Riedel, R., Dressler, W. and Reichert, S., Thermal decomposition of poly(methylsilsesquicarbodiimide) to amorphous Si–C–N ceramics. *Chem. Mater.*, 1999, **11**(2), 412–420.
46. Müller, A., Peng, J., Seifert, H. J., Bill, J. and Aldinger, F., Si–B–C–N ceramic precursors derived from dichlorodivinylsilane and chlorotrivinylsilane. 2. Ceramization of polymers and high-temperature behavior of ceramic materials. *Chem. Mater.*, 2002, **14**(8), 3406–3412.
47. Schmidt, W. R., Narsavage-Heald, D. M., Jones, D. M., Marchetti, P. S., Raker, D. and Maciel, G. E., Poly(borosilazane) precursors to ceramic nanocomposites. *Chem. Mater.*, 1999, **11**(6), 1455–1464.
48. Ginzburg, M., MacLachlan, M. J., Yang, S. M., Coombs, N., Coyle, T. W., Raju, N. P. *et al.*, Genesis of nanostructured, magnetically tunable ceramics from the pyrolysis of cross-linked polyferrocenylsilane networks and formation of shaped macroscopic objects and micron scale patterns by micromolding inside silicon wafers. *J. Am. Chem. Soc.*, 2002, **124**(11), 2625–2639.
49. Sun, Q., Lam, J. W. Y., Xu, K., Xu, H., Cha, J. A. K., Wong, P. C. L. W. *et al.*, Nanocluster-containing mesoporous magnetoceramics from hyperbranched organometallic polymer precursors. *Chem. Mater.*, 2000, **12**(9), 2617–2627.
50. Johnson, S. A., Ollivier, P. J. and Mallouk, T. E., Ordered mesoporous polymers of tunable pore size from colloidal silica templates. *Science*, 1999, **283**, 963–965.
51. Popielarz, R., Chiang, C. K., Nozaki, R. and Obrzut, J., Dielectric properties of polymer/ferroelectric ceramic composites from 100 Hz to 10 GHz. *Macromolecules*, 2001, **34**(17), 5910–5915.
52. Mansky, P., Liu, Y., Huang, E., Russell, T. P. and Hawker, C., Controlling polymer–surface interactions with random copolymer brushes. *Science*, 1997, **275**, 1458–1460.
53. Ingall, M. D. K., Honeyman, C. H., Mercure, J. V., Bianconi, P. A. and Kunz, R. R., Surface functionalization and imaging using monolayers and surface-grafted polymer layers. *J. Am. Chem. Soc.*, 1999, **121**(15), 3607–3613.
54. Venkataraman, A., Hiremath, V. A., Date, S. K. and Kulkarni, S. D., A new combustion route to γ-Fe_2O_3 synthesis. *Bull. Mater. Sci.*, 2001, **24**(6), 617–621.
55. (a) Eilers, H., The viscosity of emulsion made of highly viscous materials as a function of the concentration. *Kolloid Z.*, 1941, **97**, 313–321;
    (b) Myers, D., *Surfaces, Interfaces, and Colloids: Principles and Applications.* VCH Publishers, New York, 1991, p. 65.
56. Jean, J.-H. and Chang, C.-R., Cofiring kinetics and mechanisms of an Ag-metallized ceramic-filled glass electronic package. *J. Am. Ceram. Soc.*, 1997, **80**(12), 3084–3092.
57. Koke, J. and Modigell, M., Flow behaviour of semi-solid metal alloys. *J. Non-Newtonian Fluid Mech.*, 2003, **112**(2–3), 141–160.
58. Sharma, P. K., Varadan, V. V. and Varadan, V. K., Effect of Tween 80 on the control of particle size and shrinkage properties of nanoscale α-alumina synthesized by sol–gel processing. *J. Am. Ceram. Soc.*, 2002, **85**(10), 2584–2586.